Criteria for the observation of strong-field photoelectron holography

T. Marchenko, Y. Huismans, K. J. Schafer, and M. J. J. Vrakking

Phys. Rev. A **84**, 053427 — Published 22 November 2011

DOI: 10.1103/PhysRevA.84.053427

Criteria for the observation of strong-field photoelectron holography

T. Marchenko[1]*, Y. Huismans[2], K.J. Schafer[3] and M. J. J. Vrakking[2,4]

[1] *UPMC Univ Paris 06, CNRS, UMR 7614, Laboratoire de Chimie Physique Matière et Rayonnement, 11 rue Pierre et Marie Curie, F-75005 Paris, France*
[2] *FOM-Institute AMOLF, Science Park 113, 1098 XG Amsterdam, The Netherlands*
[3] *Department of Physics and Astronomy, Louisiana State University, Baton Rouge, Louisiana 70803-4001, USA*
[4] *Max-Born-Institut, Max Born Straße 2A, D-12489 Berlin, Germany*

Photoelectron holography is studied experimentally and computationally using the ionization of ground state xenon atoms by intense near-infrared radiation. A strong dependence of the occurrence of the holographic pattern on the laser wavelength and intensity is observed, and it is shown that the observation of the hologram requires that the ponderomotive energy U_p is substantially larger than the photon energy. The holographic interference is therefore favored by longer wavelengths and higher laser intensities. Our results indicate that the tunneling regime is not a necessary condition for the observation of the holographic pattern, which can be observed under the conditions formally attributed to the multi-photon regime.

I. INTRODUCTION

Ionization of atoms or molecules in a strong laser field leads to the emission of coherent electron wave packets that propagate in the combined Coulomb and laser field. Electrons that are ionized at different times within the laser pulse and that eventually acquire the same final momentum, give rise to interference. The first observation of photoelectron interference was in the well-known phenomenon of above-threshold ionization (ATI) [1]. In the time domain, ATI originates from the interference of electron wave packets emitted from the atom at time intervals separated by the optical period of the laser. In the energy domain ATI is commonly considered as a result of the absorption by the atom of a number of photons in excess of the minimum required to reach the ionization threshold, with a corresponding photoelectron spectrum containing peaks separated by the energy of a single photon.

Another type of photoelectron interference was observed with few-cycle carrier-envelope phase stabilized laser pulses [2, 3]. The propagation of electron wave packets launched in adjacent

* tatiana.marchenko@upmc.fr

half-cycles at the same, but opposite value of the laser electric field (and, hence, at the same value of the vector potential $(A(t) = \int E(t)dt)$ leads to the emergence of pairs of electron trajectories that start on opposite sides of the ion and that either go to the detector directly or after turning around under the influence of the laser field. This interference can be considered as a time double-slit interference [4], which produces structures in the photoelectron energy spectrum that are qualitatively different from the regular ATI peaks observed with longer pulses. Ionization at the positive or negative peak of the laser electric field (where the ionization rate is maximal, and where the $A(t)=0$) leads to the creation of electrons that acquire only a very small momentum under the influence of the laser field. Influenced by the long-range Coulomb interaction, the interference of these electron wave packets, which are ionized at time-intervals corresponding to half the optical period of the laser, leads to a radial pattern in the electron momentum distribution below the first ATI order [5, 6, 7], which persists also for long pulses containing many cycles.

Recently, a new type of photoelectron interference was reported, which originates from the interference of electron wave packets born within the same quarter cycle of the laser pulse [8]. In this case the interference arises from two trajectories that start on the same side of the ion and that interact with the ionic potential, however in a quantitatively drastically different way. One trajectory undergoes strong Coulomb focusing and passes close to the ion, whereas the other trajectory is only weakly affected by the Coulomb field and makes a wide turn around the ion. The resulting interference pattern contains fringes in the electron angular distributions and can be considered as a hologram of the scattering potential. The first results reported on the observation of these holographic patterns in photoelectron imaging spectroscopy were obtained under very specific conditions. The experiment was performed on metastable (6s) xenon atoms that were ionized with 7 μm mid-infrared free-electron laser (FEL) radiation. The combination of long-wavelength radiation with the low binding energy of the ionized atom provided very favorable conditions for the observation of the hologram. Furthermore, the importance of ionization in the tunneling regime for the appearance of the holographic pattern was assumed. The required and sufficient conditions for the observation of a photoelectron hologram were not yet investigated in this work.

Here we explore photoelectron holography over a broad range of laser parameters, by varying the laser intensity and wavelength and thereby encompassing both the tunneling and multi-photon regimes of ionization. We present experimental observations for the strong-field ionization of xenon atoms in the ground state with near-infrared radiation in the wavelength range between 600 and 800 nm and between 1200 and 1600 nm. These experimental results are quantitatively compared with the results of calculations solving the time-dependent Schrödinger Equation (TDSE), with a full integration over the laser focal volume. Extending our calculations over a significantly broader range of parameters than available in the experiments, we explore the dependence of the holographic pattern on the laser wavelength and intensity, and show that the possibility to observe the hologram exists

both in the tunneling and the multi-photon regimes. An empirical criterion for the laser parameters that allow the observation of a hologram is established.

II. EXPERIMENTAL AND THEORETICAL METHODS

In the experiment, a commercial laser system consisting of an optical parametric amplifier (OPA, *Coherent Opera*) pumped by 1 mJ from a 1 kHz Ti:Sapphire amplifier system (800 nm, 50 fs) was used. The OPA signal output provided pulses with a wavelength in the range from 1200 to 1600 nm with a FWHM of 10-15 nm. Frequency doubling of the OPA output using a BBO crystal provided pulses with a wavelength in the range from 600 to 800 nm. The central wavelength was determined with an accuracy of 2 nm using a spectrometer. The linearly polarized laser beam was focused onto a pulsed atomic beam (25 Hz) using a spherical normal-incidence silver mirror (f=75 mm). The ejected electrons were detected using a Velocity Map Imaging (VMI) spectrometer [9], consisting of a set of acceleration electrodes, a flight tube, a dual MCP and a phosphor screen. Images were recorded using a computer-controlled CCD camera. Retrieval of the velocity and angular distribution of the measured photoelectrons was performed by using an iterative inverse Abel transform procedure of [10]. Slices through the 3D velocity and angular distribution of the ionized electrons are referred to in the following as momentum maps.

Experimental images were obtained by summing the electron yield over five minutes of acquisition time. In order to explore the evolution of the momentum maps with the laser wavelength, photoelectron momentum maps were recorded in xenon over a range of wavelengths from 1200 – 1600 nm, and from 600 – 800 nm, while attempting to keep the laser intensity constant using the observation of the ratio of double-to-single ionization in an ion time-of-flight measurement as a rough indicator. In the analysis the experimental intensities were deduced by comparing the measured results to numerical solutions of the 3D TDSE within the single-active electron (SAE) approximation [11], i.e. considering only the response of the outermost valence electron to the laser field. In order to solve the TDSE for xenon we used a code based on the method outlined in [12, 13] with a pseudo-potential described in [14]. The code provides energy-resolved electron angular distributions [15], which can be converted into a 2D momentum map that allows comparison with the experimentally recorded images. For an adequate comparison to the experiment, the results of the TDSE calculations were integrated over the laser focal volume with the assumption of a Gaussian beam profile and a width of the target beam much smaller than the Rayleigh range [16]. The temporal profile of the laser pulse was modeled with a sine-squared envelope typically containing 20 optical cycles. In our discussion, atomic units ($e=m_e=\hbar=1$) will be used throughout, unless mentioned otherwise.

III. RESULTS AND DISCUSSION

FIG. 1 and FIG. 2 show a series of momentum maps at wavelengths from 1200 - 1600 nm and from 600 - 800 nm, where experimental images presented on the left are compared to TDSE results on the right. The peak laser intensity used in the calculations was chosen to provide the best agreement with the experimental data (based on visual inspection) and remained on average around $3\text{-}6\times10^{13}$ W/cm^2 with an estimated error of less than 5% in the individual intensities. These experimental conditions are in the multi-photon regime for the 600-800 nm results and correspond to the transition region between the multi-photon and the tunneling regime for the 1200-1600 nm results, where we make use of the convention to define the transition between the multi-photon and tunneling regimes as the point where the Keldysh parameter $\gamma = \left(IP/2U_p\right)^{1/2} \approx 1$, where *IP* is the ionization potential and $U_p = F_0^2/4\omega^2$ is the electron ponderomotive energy in a laser field with the amplitude F_0 and frequency ω. The dominant contribution peaking along the laser polarization axis in the momentum maps presented in FIG. 1 and FIG. 2 corresponds to ATI [1]. Away from the laser polarization axis the photoelectron momentum maps in FIG. 1 and FIG. 2 show a significant qualitative difference. At the infrared wavelengths between 1200 and 1600 nm (FIG. 1), the momentum maps are dominated by cross-like sidelobes extending from the center of the image and marked with a black dashed line in Fig. 1 (a). These sidelobes are qualitatively similar to the holographic patterns observed in [8] and can be attributed to the interference of electron wave packets originating from the same quarter-cycle of the laser pulse. In contrast, the holographic pattern is absent in the momentum maps at the visible wavelengths between 600 and 800 nm (FIG. 2). The qualitative difference between the photoelectron momentum maps at the visible and the infrared wavelengths raises the question what the criteria are for the observation of strong-field photoelectron holography. In order to explore this question the evolution of the holographic pattern with the laser wavelength and intensity will be analyzed on the basis of computational results that are in good agreement with the experiment, but that can be studied over a wider range of parameters than is accessible in the experiment.

Extending the experimentally available wavelength range, FIG. 3 shows a series of calculated momentum maps at various laser wavelengths between 4560 and 400 nm and at a constant value of the ponderomotive energy U_p=0.2 a.u. (5.44 eV), corresponding to a Keldysh parameter $\gamma\approx1$. In order to quantify the visibility of the holographic pattern, we introduce a parameter $R=I_{min}/I_{max}$, where I_{min} and I_{max} are the first minimum and maximum encountered in the p_x momentum distribution when going away from the laser polarization at a constant $p_y = \frac{1}{2} p_{y\_cut-off}$, with $p_{y\_cut-off} = 2\sqrt{U_p}$ being the momentum corresponding to the $2U_p$ cut-off in energy. In the following a holographic pattern is considered visible when R<0.85. The holographic pattern is clearly visible at the long laser wavelengths (FIG. 3(a), (b)) and gradually washes out towards the shorter wavelengths. In this

intensity regime a hint of the holographic pattern can still be identified at wavelengths as short as 650 nm.

Our results indicate that the appearance of the holographic interference is strongly dependent on the laser wavelength range considered. On the other hand, the range of wavelengths where the holographic interference can be observed depends on the intensity regime. This is demonstrated in FIG. 4, which shows a series of calculated photoelectron momentum maps at a fixed wavelength of 1840 nm and at various peak intensities spanning the range of the Keldysh parameter $0.8<\gamma<3$. The holographic pattern is not present in the momentum maps at the lowest intensity of 0.2×10^{13} W/cm^2 (FIG. 4 (a)), but dominates the spectra at the higher intensities (FIG. 4 (b)-(d)). The appearance of the holographic pattern at reduced laser intensities (or at reduced ponderomotive energies) requires the involvement of increasingly longer wavelengths. Note that the holographic interference reported in [8] was observed at laser intensities of $10^{11} - 10^{12}$ W/cm^2 and a wavelength of 7μm.

Interestingly, the onset of the holographic pattern in FIG. 4 occurs at a peak laser intensity of 1.1×10^{13} W/cm^2, where the Keldysh parameter $\gamma=1.3$, i.e. at an intensity that would typically still be considered to be part of the multi-photon regime. The transition to the tunneling regime ($\gamma=1$) at the intensity of 1.9×10^{13} W/cm^2, does not cause any qualitative change to the holographic pattern. These calculations show that the holographic interference can be clearly observed in the multi-photon regime, before the formal transition to the tunneling regime. The coexistence of multi-photon and tunneling ionization mechanisms in the parameter region near $\gamma=1$ has been discussed by Ivanov et al. [17]. Near $\gamma=1$ the barrier in the combined Coulomb and laser field potential through which the electron tunnels, changes significantly during tunneling. Therefore one cannot determine unambiguously, whether multi-photon or tunneling ionization is responsible for the holographic pattern at the region where $\gamma\sim1$.

A diagram in FIG.5 provides an overview of the laser parameters explored in our present experimental and computational study including computational data not shown in Figures 1-4. The filled symbols in the diagram correspond to photoelectron momentum maps where the holographic pattern can be observed, whereas open symbols indicate the absence of the pattern. A solid horizontal line at $U_p= 6$ eV marks the formal transition from the multi-photon to the tunneling regime, when the Keldysh parameter goes through unity. One can observe that the holographic pattern can be predominantly observed at long wavelengths in the near- to mid-infrared range (filled symbols in FIG.5). In this wavelength range the observation of the holographic interference requires moderate laser intensities (and moderate ponderomotive electron energies) close to the transition from the multi-photon to the tunneling regime. However, shortening of the laser wavelength leads to a gradual vanishing of the holographic pattern from the momentum maps (empty symbols).

As indicated earlier in [8] and demonstrated in the diagram in FIG.5 a large ponderomotive energy of the ionized electron with respect to the photon energy (i.e. $U_p/\omega >>1$) is a crucial

requirement for the holographic interference. Consequently, the laser parameters favorable for the observation of the holographic interference tend favorably towards longer wavelengths and higher intensities. Our results confirm that generally a hologram can be clearly observed when $U_p/\omega > 4$. On one hand the dimensionless parameter U_p/ω defines the applicability of perturbation theory [18], i.e. the holograms are not observed under perturbative conditions. On the other hand U_p/ω is the number of photons required to allow an electron to be a free particle in the presence of a strong laser field [19]. Both aspects point towards the important role of the strong laser field in establishing the conditions for the observation of the hologram, which is, after all, caused by the interference between electrons that re-scatter (under the influence of the laser field) and electrons that do not re-scatter but that are also turned around by the laser field.

IV. CONCLUSION

In conclusion, we have experimentally demonstrated photoelectron holography in ground state xenon ionized by intense near-infrared radiation. Our calculations demonstrate a strong dependence of the holographic pattern on the laser wavelength and intensity and show that the condition $U_p/\omega >> 1$ is crucial for the holographic interference, which therefore can be favorably observed at longer wavelengths and higher laser intensities. Our results indicate that the tunneling regime is not a necessary condition for the observation of the holographic pattern. The signature of the holographic interference can be observed under the conditions formally attributed to the multi-photon regime ($\gamma > 1$).

ACKNOWLEDGMENTS

This work is part of the research program of the "Stichting voor Fundamenteel Onderzoek der Materie" (FOM), which is financially supported by the "Nederlandse Organisatie voor Wetenschappelijk Onderzoek" (NWO). KJS is supported by National Science Foundation Grant No. PHY-0701372.

References

[1] P. Agostini, F. Fabre, G. Mainfray, G. Petite, and N. K. Rahman, Phys. Rev. Lett. **42,** 1127 (1979)

[2] R. Gopal *et al.*, Phys. Rev. Lett. **103,** 053001 (2009)

[3] F. Lindner *et al.,* Phys. Rev. Lett. **95,** 040401 (2005)

[4] D. G. Arbó, E. Persson and J. Burgdörfer, Phys. Rev. A **74,** 063407 (2006)

[5] A. Rudenko, K. Zrost, C. D. Schroter, V. L. B. de Jesus, B. Feuerstein, R. Moshammer, and J. Ullrich, J. Phys. B: At. Mol. Opt. Phys. **37,** L407 (2004)

[6] D. G. Arbó, K. I. Dimitriou, E. Persson and J. Burgdörfer, Phys. Rev. A **78,** 013406 (2008)

[7] T. Marchenko, H. G. Muller, K. J. Schafer and M. J. J. Vrakking, J. Phys. B: At. Mol. Opt. Phys. **43,** 095601 (2010)

[8] Y. Huismans *et al.,* Science **331,** 61 (2011)

[9] A. T. J. Eppink and D. H. Parker, Rev. Sci. Instrum. **68,** 3477 (1997)

[10] M. J. J. Vrakking, Rev. Sci. Instrum. **72,** 4084 (2001)

[11] K. C. Kulander, K. J. Schafer and J. L. Krause, in *Atoms in Intense Laser Fields,* edited by M. Gavrila (New York: Academic Press, 1992)

[12] K. J. Schafer and K. C. Kulander, Phys. Rev. A **42,** 5794 (1990)

[13] K. J. Schafer, in *Strong Field Laser Physics*, edited by T. Brabec (New York: Springer Science + Business Media, 2008)

[14] K. C. Kulander and T. N. Rescigno, Comput. Phys. Commun. **63,** 523 (1991)

[15] K. J. Schafer, Comput. Phys. Commun. **63,** 427 (1991)

[16] J. H. Posthumus, Rep. Prog. Phys. **67,** 623 (2004)

[17] M. Yu. Ivanov, O. Smirnova and M. Spanner, J. Mod. Opt. **52,** 165 (2005)

[18] H. R. Reiss, Phys. Rev. A **22,** 1786 (1980)

[19] H. R. Reiss, Phys. Rev. Lett. **102,** 143003 (2009)

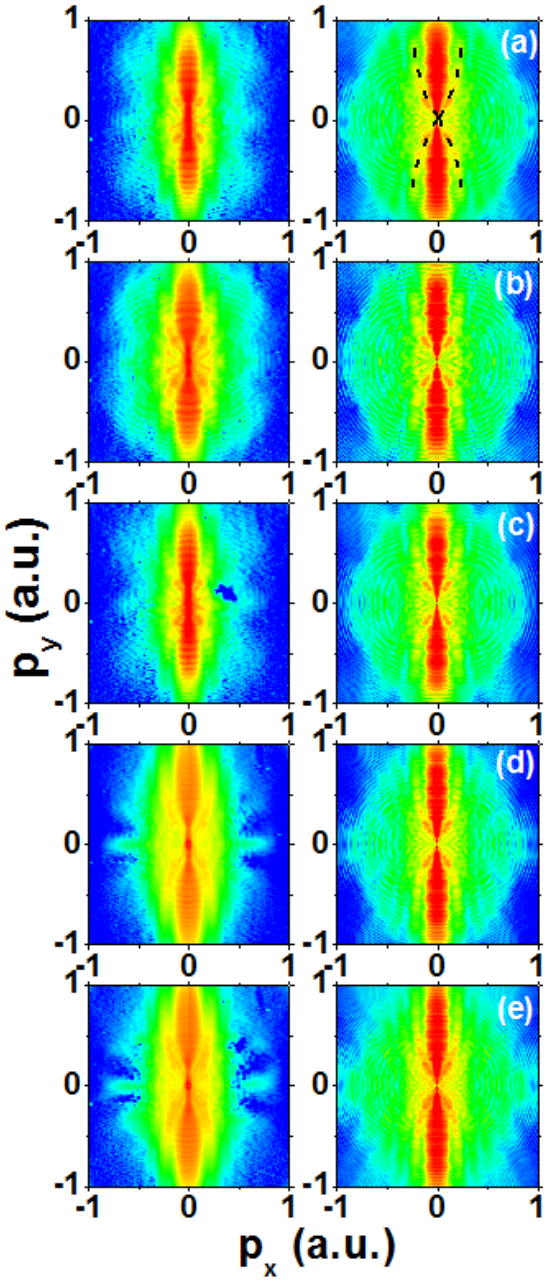

FIG. 1. (Color online) Experimental (left column) and calculated (right column) momentum maps for ionization of xenon at various wavelengths and intensities: (a) 1200 nm, 4.3×10^{13} W/cm^2, γ=1.03; (b) 1300 nm, 4.2×10^{13} W/cm^2, γ=0.96; (c) 1375 nm, 3.1×10^{13} W/cm^2, γ=1.05; (d) 1475 nm, 3.3×10^{13} W/cm^2, γ=0.94; (e) 1575 nm, 3.4×10^{13} W/cm^2, γ=0.87. The logarithmic false-color scale covers three orders of magnitude. The holographic pattern is marked in (a) with a black dashed line.

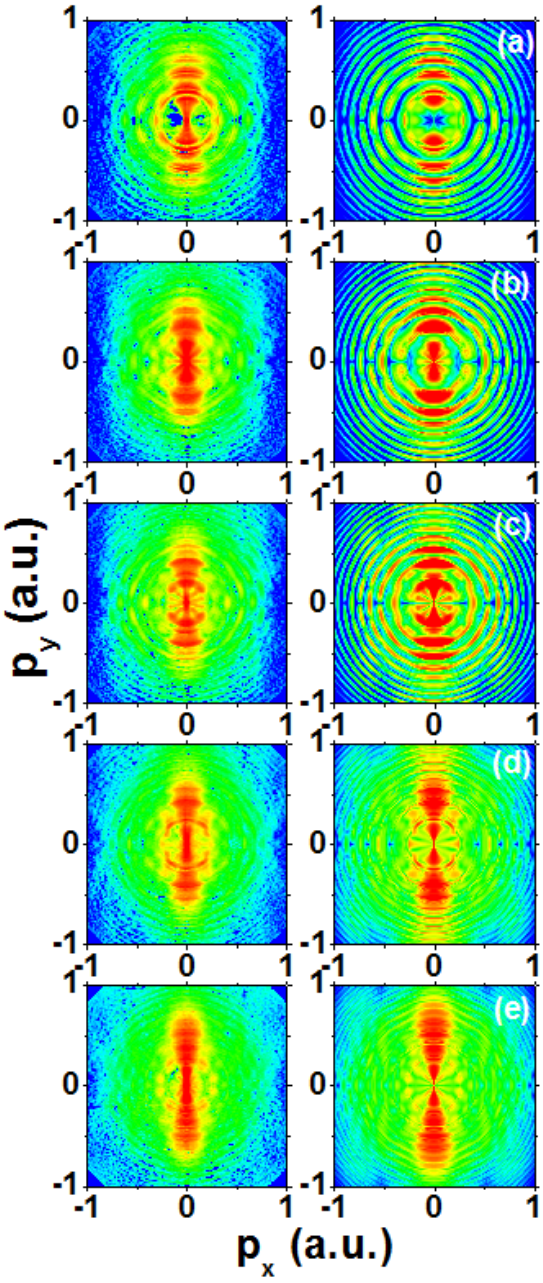

FIG. 2. (Color online) Experimental (left column) and calculated (right column) momentum maps for ionization of xenon at various wavelengths and intensities: (a) 600 nm, 5.7×10^{13} W/cm^2, γ=1.78; (b) 650 nm, 4.6×10^{13} W/cm^2, γ=1.83; (c) 700 nm, 4.5×10^{13} W/cm^2, γ=1.72; (d) 740 nm, 6.4×10^{13} W/cm^2, γ=1.36; (e) 800 nm, 6.7×10^{13} W/cm^2, γ=1.23. The logarithmic false-color scale covers four orders of magnitude.

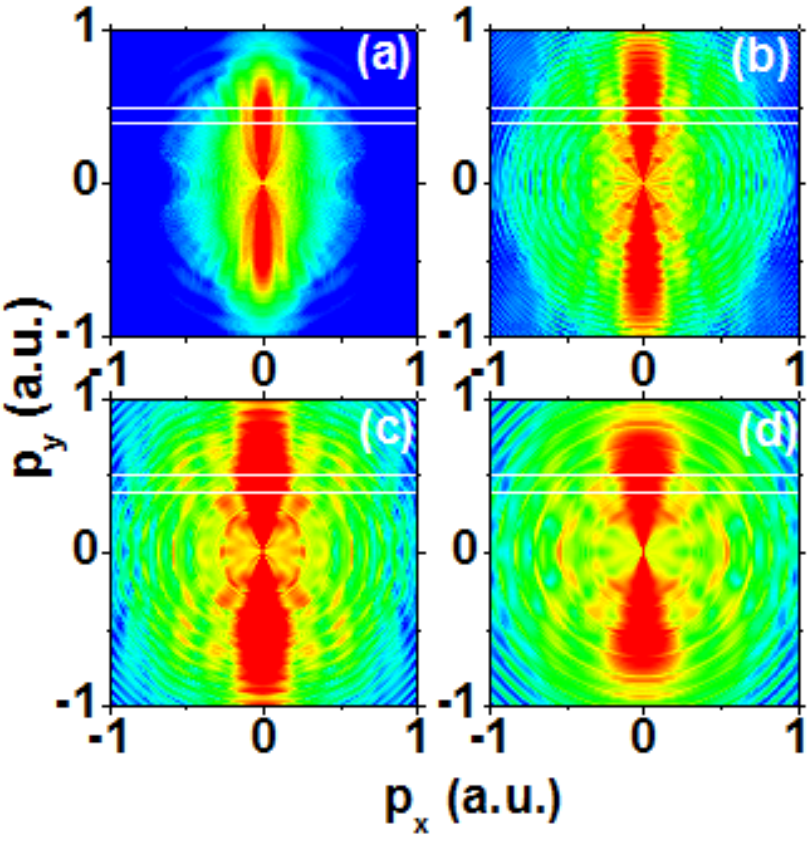

FIG. 3. (Color online) Calculated momentum maps for ionization of xenon at U_p=5.44 eV and various wavelengths: (a) 4560 nm, 0.3×10^{13} W/cm^2, R=0.78; (b) 1140 nm, 4.5×10^{13} W/cm^2, R=0.76; (c) 650 nm, 1.4×10^{14} W/cm^2, R=0.86; (d) 460 nm, 2.8×10^{14} W/cm^2, R=0.91. The logarithmic false-color scale covers three orders of magnitude. The horizontal white lines mark the momentum p_y where the parameter R is calculated.

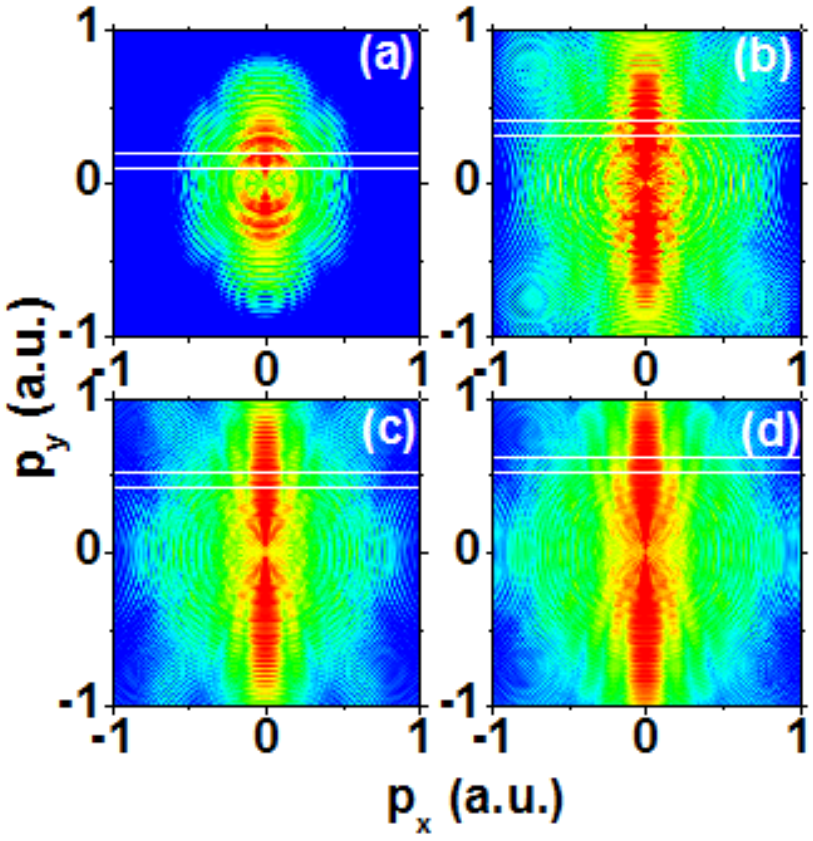

FIG. 4. (Color online) Calculated momentum maps for ionization of xenon at λ=1840 nm and various intensities: (a) 0.2×10^{13} W/cm^2, γ=3.1, R=0.89; (b) 1.1×10^{13} W/cm^2, γ=1.3, R=0.71; (c) 1.9×10^{13} W/cm^2, γ=1, R=0.63; (d) 2.8×10^{13} W/cm^2, γ=0.8, R=0.51. The logarithmic false-color scale covers three orders of magnitude. The horizontal white lines mark the momentum p_y where the parameter R is calculated.

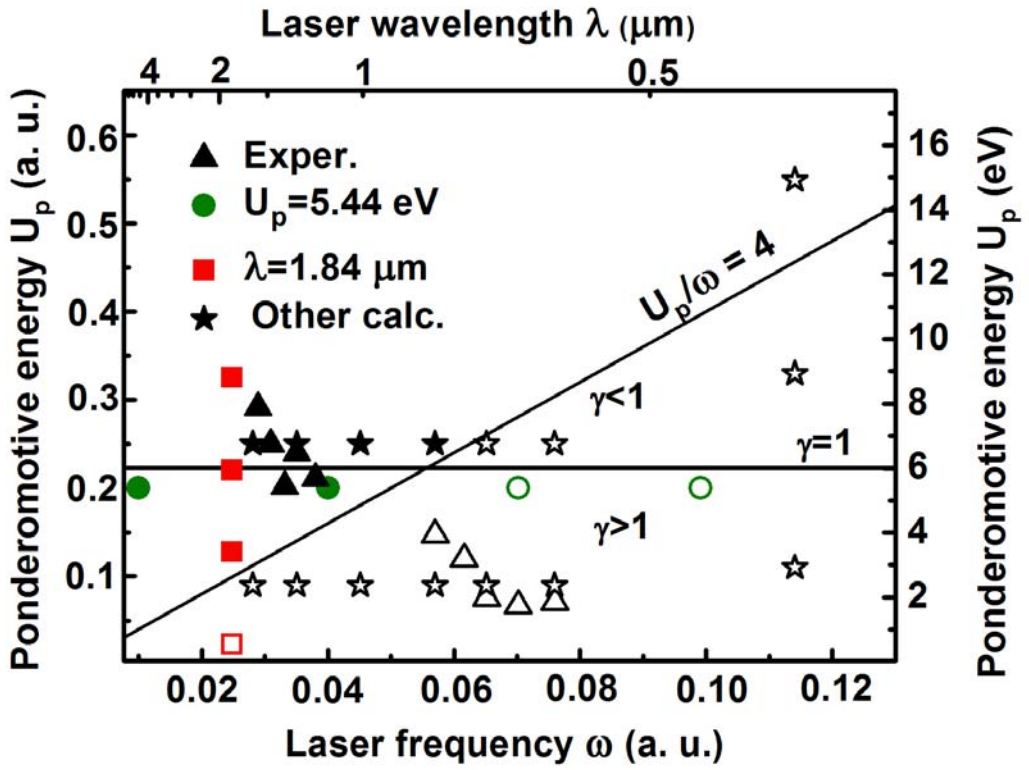

FIG.5. (Color online) A diagram showing the range of laser parameters explored in this paper. The filled and empty symbols correspond respectively to the presence and absence of the holographic pattern in the momentum maps, shown in the previous figures. A solid horizontal line at U_p= 6 eV marks the formal transition from the multi-photon to the tunneling regime, when the Keldysh parameter goes through unity. Note that care must be taken with the interpretation of the results at short wavelengths and high intensity, since enhancement of intensity above the saturation of singly-charged xenon ion yield may lead to depletion of the ground state before the tunneling regime can be reached.